Quasiparticle and hybrid density functional methods in defect studies: An application to the nitrogen vacancy in GaN

D. K. Lewis, M. Matsubara, E. Bellotti, and S. Sharifzadeh

Phys. Rev. B **96**, 235203 — Published 18 December 2017

DOI: 10.1103/PhysRevB.96.235203

Quasiparticle and Hybrid Density Functional Methods in Defect Studies: An Application to the Nitrogen Vacancy in GaN

D.K. Lewis,[1] M. Matsubara,[1] E. Bellotti,[1,2] S. Sharifzadeh[1,2,3]

[1]Department of Electrical and Computer Engineering, Boston University, Boston, MA 02215

[2]Division of Materials Science and Engineering, Boston University, Boston, MA 02215

[3] Department of Physics, Boston University, Boston, MA 02215

Abstract

Defects in semiconductors can play a vital role in the performance of electronic devices, with native defects often dominating the electronic properties of the semiconductor. Understanding the relationship between structural defects and electronic function will be central to the design of new high-performance materials. In particular, it is necessary to quantitatively understand the energy and lifetime of electronic states associated with the defect. Here, we apply first-principles density functional theory (DFT) and many-body perturbation theory within the GW approximation to understand the nature and energy of the defect states associated with a charged nitrogen vacancy on the electronic properties of gallium nitride (GaN), as a model of a well-studied and important wide gap semiconductor grown with defects. We systematically investigate the sources of error associated with the GW approximation and the role of the underlying atomic structure on the predicted defect state energies. Additionally, analysis of the computed electronic density of states (DOS) reveals that there is one occupied defect state 0.2 eV below the valence band maximum and three unoccupied defect states at energy of 0.2-0.4 eV above the conduction band minimum, suggesting that this defect in the +1 charge state will not behave as a carrier trap. Furthermore, we compare the character and energy of the defect state obtained from GW and DFT using the HSE approximate density functional, and find excellent agreement. This systematic study provides a more complete understanding of how to obtain quantitative defect energy states in bulk semiconductors.

I. Introduction

The presence of defects strongly influences semiconductor electronic and optical properties[1–3] and can significantly alter their optoelectronic device behavior. Defects can modify material properties, as with defect-mediated dopant diffusion[4] or the formation of defect levels deep in the band gap, which behave as carrier trapping and recombination centers[5] and facilitate undesirable low-energy photoluminescence in light-emitting materials[6]. In particular, native point defects are an important and pervasive class of semiconductor defects, which can occur in a variety of charge states and can dominate optoelectronic properties[7,8]. In order to understand their influence, it is necessary to determine the type and charge state of the defect, and how these features influence the atomic and electronic structure of the semiconductor. Although such properties can be probed via experimental techniques such as electron paramagnetic resonance, vibrational spectroscopy, capacitance, and photoluminescence measurements[6], there are many situations where experiment alone has not been sufficient, necessitating theory and computation[8–11].

First-principles electronic structure methods, particularly density functional theory (DFT), have enabled the mapping of measurable quantities to a particular defect geometry and charge state in an unambiguous fashion, providing information complimentary to measurements. DFT-based studies have often focused on calculating defect formation energies for different charge states[12,13]; the predicted defect energetics, thermodynamic transition levels, and associated configuration

coordinate diagrams determined from such analyses have played an important role in understanding electrical and optical properties of important optoelectronic semiconductors such as Si[14–17], GaAs[18–25], and GaN[5,26–33]. These computational studies have provided a significant insight into defect identification, structural properties near defects, and the cause of low-energy luminescence in defective materials.

In order to describe electron transport within defective semiconductors, it is additionally necessary to quantitatively describe trap states, i.e. the energy required to add or remove an electron from an electronic state associated with a given defect. Conventional electronic device modeling represents defects as simple trap-like models, with a given trap energy and lifetime associated with the defect state. The inclusion of a more sophisticated description of defects is required to understand how defects impact device performance and reliability. This will require the ability to determine from first-principles the energy of the defect state relative to the valence and conduction band edges, and the associated time constants, as well as the development of new device simulation models that can effectively utilize this information[34].

Kohn-Sham DFT (KS-DFT) provides orbital energies that can approximate the defect state energy and lifetime. However, the orbital energies obtained within standard approximations to KS-DFT are not necessarily accurate when compared against physically observed addition and removal energies, in part due to the well-known self-interaction and derivative discontinuity errors[35,36]. To improve upon standard DFT, hybrid DFT functionals within generalized Kohn-Sham DFT, such as that of Heyd, Scuseria & Ernzerhof (HSE)[37] have been utilized to predict accurate band gaps[38]. Additionally, it has been shown that by tuning the HSE functional to reproduce the experimental bulk band gaps, the defect transition energetics relative to the band gap edges can be more accurately predicted. Such a tuned HSE functional has provided increased insight into a number of different defects[28,29,39–47]. However, the physical justification for the tuning is unclear[41,48,49] and there is no guarantee that both delocalized bulk-like and localized defect-type states will be treated with equal accuracy using this approach.

Alternatively, many-body perturbation theory (MBPT) within the GW approximation can accurately predict band gaps and addition/removal energies for many materials classes from first principles with no empirical tuning of parameters[50–52]. The GW approximation, by including electron-electron interactions within first-order perturbation theory, provides a first-principles approach that does not suffer from self-interaction or derivative discontinuity errors, and treats bulk and defect states at the same level of accuracy. However, the GW approximation can come at a significant computational cost depending upon the details of the particular implementation, and thus this technique has been applied to relatively few with-defect solids compared to strictly DFT-based approaches. The GW approach has been successfully applied to defects, resulting in better agreement with experiment than DFT for defect formation energies[53], thermodynamic transition levels[54–57], and photoluminescence lines[54]. In purely theoretical studies, application of the GW approach to defects has provided significant insight into the role of many-body interactions on defect energies[58–63].

In this study, we apply the GW approximation to quantitatively determine the energy of defect states associated with a charged nitrogen vacancy in bulk GaN as a prototypical defective system, and carefully compare with the results of DFT-HSE. GaN is known to grow with significant defect concentrations that degrade its performance in optoelectronic applications[43,64], and as such has been widely studied both computationally and experimentally[5,6,10,65]. Point defects such as nitrogen vacancies are expected to significantly degrade device performance[5] by introducing mid-gap states that behave as carrier trapping and recombination centers and result in undesirable low-energy photoluminescence[6]. Measurements have shed light on the energy of the trap state associated with point defects within GaN[10,66,67]; however relatively few have been unambiguously mapped to a particular defect geometry and charge state. While many point defects and complexes within GaN have been studied, no in depth analysis of the nature of the defect state has been presented.

We investigate, for the first time, the electronic structure of defective wurtzite GaN containing the nitrogen vacancy point defect in the 1+ charge state (V_N^{1+}) within the GW approximation. Importantly, we systematically investigate the role of

geometry and defect-defect interactions on predicted defect energies. We determine that GW and DFT-HSE agree very well in terms of the character of the defect state and its energy. Analysis of the computed electronic density of states (DOS) reveals that there is one occupied s-like and three unoccupied p-like states localized near the defect, with energies close to the band edges of GaN, and that there are a number of orbitals of a hybrid bulk- and defect-like character that modify the DOS compared with the pristine bulk. Moreover, we determine the error associated with different approximations, including the underlying structure of the GaN. For the pristine bulk, different geometry optimization techniques utilizing different DFT functionals result in predicted band gaps that can vary by as much as 0.8 eV. With the presence of the defect, the relative defect energy with respect to band edges is also strongly influenced by the underlying geometry by up to 0.2 eV. Our systematic study provides a more complete understanding of how to obtain quantitative defect energy states in bulk semiconductors.

II. Computational Details

II.1 Geometry Optimization of Pristine and With-Defect Structures

The structure of the pristine wurtzite bulk structure and the with-defect supercell were optimized within DFT using two different density functionals, the local density approximation (LDA)[68] and the Heyd-Scuseria-Ernzerhof (HSE)[37,69]. The pristine bulk GaN geometry was optimized by relaxing the atomic positions, lattice constants, and crystal shape. To describe an isolated defect within the bulk, we 1) created an n x n x m supercell; 2) re-optimized the bulk geometry within this supercell; 3) removed a nitrogen atom from the supercell such that the vacancy created is as symmetric as possible with respect to the supercell geometry; 4) removed one electron from the system in order to simulate the +1 charge state; and 5) optimized atomic positions in the presence of the defect. For charged defects, a compensating background charge was applied in order to avoid a divergent Coulomb energy for the periodically repeated supercell[70].

DFT-HSE calculations were performed using the VASP package[71,72], while DFT-LDA calculations were performed using the Quantum Espresso software package[73]. Bulk unit cell (supercell) geometries were optimized with a Brillouin zone sampling of 8x8x8 (2x2x2), which was found sufficient to converge the total energy to less than 1 meV/atom, with a force threshold of 0.03 eV/Å for the LDA calculation and 0.05 eV/Å for the HSE calculation. To lessen computational cost, we explicitly treated 3 and 5 electrons as valence for Ga and N, respectively. For VASP calculations, projector augmented wave (PAW) potentials described the core and nuclei[74], with a planewave cutoff of 31 Ry, while LDA calculations within the Quantum Espresso software package were performed with the core and nuclei of atoms described by Troullier-Martins norm-conserving pseudopotentials[75], with non-linear core correction (NLCC)[76] applied to compensate for lack of core electrons in Ga. The cutoff radii were 1.9, 2.0 and 2.8 a.u. for the s, p and d-channels respectively, for the Ga pseudopotential, and 1.3 and 1.6 a.u. for the s and p-channels respectively, for N. A planewave energy cutoff of 220 Ry was used for geometry optimization, converging the total energies to less than 1meV/atom, while 60 Ry was used for obtaining the electronic energies, sufficient to converge Kohn-Sham energies to less than 21 meV/atom.

TABLE I. Comparison of calculated lattice constants, band gap, and valence band width (VBW) predicted using two different Ga pseudopotentials. The 3-electron pseudopotential uses the non-linear core correction (NLCC). The GW calculation uses the static remainder method for the quasiparticle energies[77].

No. of electrons in Pseudopotential	Planewave cutoff	Lattice constant		Band gap	VBW	GW band gap	GW VBW
		a	c				
	(Ry)	(Å)	(Å)	(eV)	(eV)	(eV)	(eV)
3	60	3.16	5.15	2.2	7.2	3.7	7.8
21	500	3.15	5.14	2.1	7.4	3.7	7.7

We tested the 3-valence electron Ga pseudopotential against one with 21 electrons as valence and found excellent agreement in predicted properties as shown in Table I . Here, the predicted fundamental gap using the two pseudopotentials agrees to 0.1 eV for both DFT-LDA and GW with an LDA starting point. Table I also shows the valence band width (VBW), the accuracy of which has been shown to be correlated with the experimental formation energy of with-defect structures[48]. The good agreement of the VBW to 0.1 eV further justifies our use of the 3-valence Ga pseudopotential.

The fraction of exact exchange used for the HSE functional was tuned in order to reproduce the experimental pristine bulk band gap[78] and fixed for the defect studies, as is a standard approach for defect-based studies[62]. We found that the fraction of exact exchange necessary to match the experimental value of 3.5 eV[79] is 30%, and as such, this functional will be labeled HSE30%. When the structure of GaN was fixed to that optimized by DFT-LDA, we determined that the original HSE06 [37] functional reproduced the band gap.

For our final calculations, the predicted bulk modulus is 199 GPa for HSE30% and 225 GPa for LDA, in good agreement with the experimental value of 210 GPa[80]. Furthermore, we predict geometries of the with-defect structure in good agreement with previous studies[81]. After introduction of the V_N^{1+} defect and subsequent relaxation, both DFT-HSE30% and DFT-LDA predict that Ga-N bond lengths in the immediate vicinity of the defect are decreased, while the Ga-Ga spacing near the vacancy is increased by approximately 0.8% (1.1%) using the LDA (HSE30%) functional. During the geometry relaxation processes, the point-group symmetry of the supercell maintained its 3-fold C_{3v} symmetry when optimizing with the LDA and HSE06 functionals; however, it was reduced to C_s point group symmetry when optimizing with HSE30%.

II.2 Quasiparticle Energies from the GW approximation

We calculate the quasiparticle energies for the bulk and with-defect supercells within the GW approximation[82] as implemented in the BerkeleyGW software package[83]. In all GW calculations, we take a standard G_0W_0 approach where the starting orbitals and eigenvalues for GW are taken from LDA and a correction applied to the energies only. We compute the static dielectric function within the random phase approximation (RPA)[52] and utilize the generalized plasmon-pole model (GPP) of Hybertsen and Louie[83] to extend the dielectric function to finite frequency. For the Ga pseudopotential, the non-linear core correction (NLCC) to the quasiparticle energies is set to zero as described in Reference[84]. This approach will be labeled "GW" for the remainder of the paper.

To generate the starting point for GW calculations in a supercell, a (0.5 0.5 0.5) shifted 2x2x2 k-point mesh and a plane-wave cutoff energy of 60 Ry were used as described in Section III.2.B. In order to generate an accurate density of states that properly describes the bulk as well as the defect states, we interpolate resulting eigenvalues onto a 4x4x4 k-point mesh. Additionally, as described in previous studies[77,83,85,86], the GW eigenvalues are strongly dependent on the energy of the highest unoccupied state used to build the dielectric function and self-energy and the dielectric function cutoff, two parameters that are inter-dependent. We performed a GW convergence study on pristine bulk GaN in order to determine these two parameters and kept them constant for the with-defect supercells. We determined that the quasiparticle energies and band gap are converged to less than 0.1 eV with a dielectric function cutoff of 20 Ry and a highest empty state energy of 5.1 Ry[87]. The number of unoccupied states that correspond to this energy were 74 for the pristine bulk unit cell and 1900, 3600, 11,000 for the 3x3x4, 4x4x3, and 6x6x4 with-defect supercells respectively. We utilized the static remainder method[77] to improve the rate of convergence with empty bands.

III. Results

III.1 The Accuracy of Computational Approaches for Pristine Bulk

The calculated band structure for pristine bulk wurtzite GaN within DFT-LDA, DFT-HSE, and the GW approximation is shown in Fig. 1. As expected, the band gap is predicted to be at the Γ-point for all levels of theory considered. DFT-LDA underestimates the gap at 2.1 eV while a GW correction leads to a predicted gap of 3.8 eV, close to the measured value of 3.5 eV[79], and to DFT-HSE30%, which has been tuned to match the experimental gap. The valence band widths agree between GW and HSE30% to 0.1 eV, at 7.6 eV and 7.5 eV, respectively. Overall, GW and HSE30% agree well in the predicted features of the band structure though there is a slight discrepancy in the predicted fundamental gap.

This discrepancy can be understood as due to the influence of the underlying geometry on the electronic structure as shown in Table II. For completeness, we include results from DFT-HSE06 (with 25% exact exchange[37]), as well as the Perdew, Burke, Erzenhoff (PBE) functional[88], both computed within the VASP package with computational parameters as described in Section II. As shown in Table II, the DFT functional used to optimize the lattice geometry can lead to errors of 0.3-2% in the lattice vectors, resulting in significant shift of the predicted band gaps (up to 0.8 eV) at the level of GW. As expected, the LDA functional underestimates bond-lengths while PBE overestimates bond-lengths; this geometry results in an overestimated (underestimated) band gap predicted by GW using the LDA (PBE) geometries. On the other hand, HSE06 and HSE30% geometries, which are in much better agreement with experiment, result in predicted GW band gaps very close to experiment. The sensitivity of the predicted band gap to bond-length can be understood as an electrostatic effect; the introduction of strain on a piezoelectric material such as GaN results in a change in the gap as described by the deformation potential[89].

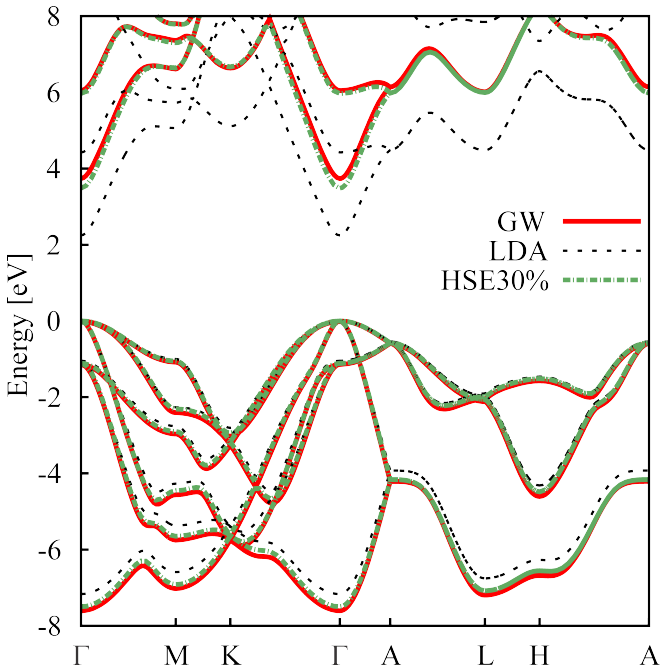

FIG. 1. The Predicted band structure for bulk wurtzite GaN within the DFT-LDA, DFT-HSE30%, and the GW approximation. The valence band maximum is shifted to zero for all plots.

As shown in Table II, if geometries are kept constant, GW and HSE06 agree quite well (to 0.2-0.3 eV). At the HSE30% geometry, where the lattice vectors agree best with experiment, GW predicts the experimental gap of 3.5 eV and agrees

exactly with HSE30%. This result indicates that, given the correct geometry, both GW and DFT using a tuned HSE functional provide an accurate description of the electronic structure of bulk GaN.

III.2 Determining Quantitatively Accurate Defect Energy States

There are significant challenges associated with defining the energy states (trap states) associated with the charged defect with respect to the bulk band edges. Here, we investigate two main challenges: the classification of defect and bulk states and minimization of defect-defect interactions.

A. Classification of the Defect State

We determine the character of the Kohn-Sham DFT orbitals by quantitative and visual examination of the charge density associated with each orbital.[1] Both DFT-LDA and DFT-HSE30% agree qualitatively as to the nature of the Kohn-Sham orbitals. These orbitals fall into three groups as shown in Fig. 2: 1) localized, defect-centered states [Fig. 2(a-b)]; 2) states that are hybrids between defect and bulk-like states [Fig. 2(c)]; and 3) states associated with sp-type Ga-N bonding in the bulk [Fig. 2(d)]. We define the defect state energy as that corresponding to the states classified by Fig. 2(a-b) because such localized states will behave as traps for carriers. However, it is important to note the presence of the hybrid states in Fig. 2(c), which suggest there is interaction of bulk electrons with the defect, which has not generally been accounted for.

TABLE II. Comparison of GW- and DFT-HSE06-predicted band gaps for bulk wurtzite GaN, with lattice vectors computed using different DFT functionals.

Functional used for Geometry Optimization	Lattice Constant		Pristine Bulk Band Gap	
			Electronic Structure Method	
	a (Å)	c (Å)	DFT-HSE06 (eV)	GW (eV)
DFT-PBE	3.25	5.28	2.8	3.0
DFT-LDA	3.16	5.15	3.5	3.8
DFT-HSE06	3.21	5.21	3.2	3.4
DFT-HSE30%	3.20	5.20	3.2	3.5
Experiment	3.19	5.19	3.5[a]	

[a] Reference[79].

For each structure, there are typically four defect-centered orbitals: one occupied s-like state in the valence band, with a spherically symmetric charge distribution strongly localized near the vacancy [Fig. 2(a)]; and three unoccupied p-like states, possessing two roughly symmetric main lobes at nearest-neighbor Ga atoms of the vacancy and separated by a nodal plane at the vacancy site [Fig. 2(b)]. Such a character to defect orbitals has been predicted previously for this

[1] We note here that while the Kohn-Sham orbitals are fictitious, they are often used to represent quasiparticle eigenstates[102], and as long as they are good representation of the quasiparticle eigenstate, the GW approximation will provide accurate quasiparticle energies.[52]

vacancy[12] and is consistent with a Hydrogenic model of the defect state. A fourth p-like state is present in the conduction band at some k-points; its presence is due to hybridization of bulk and defect states.

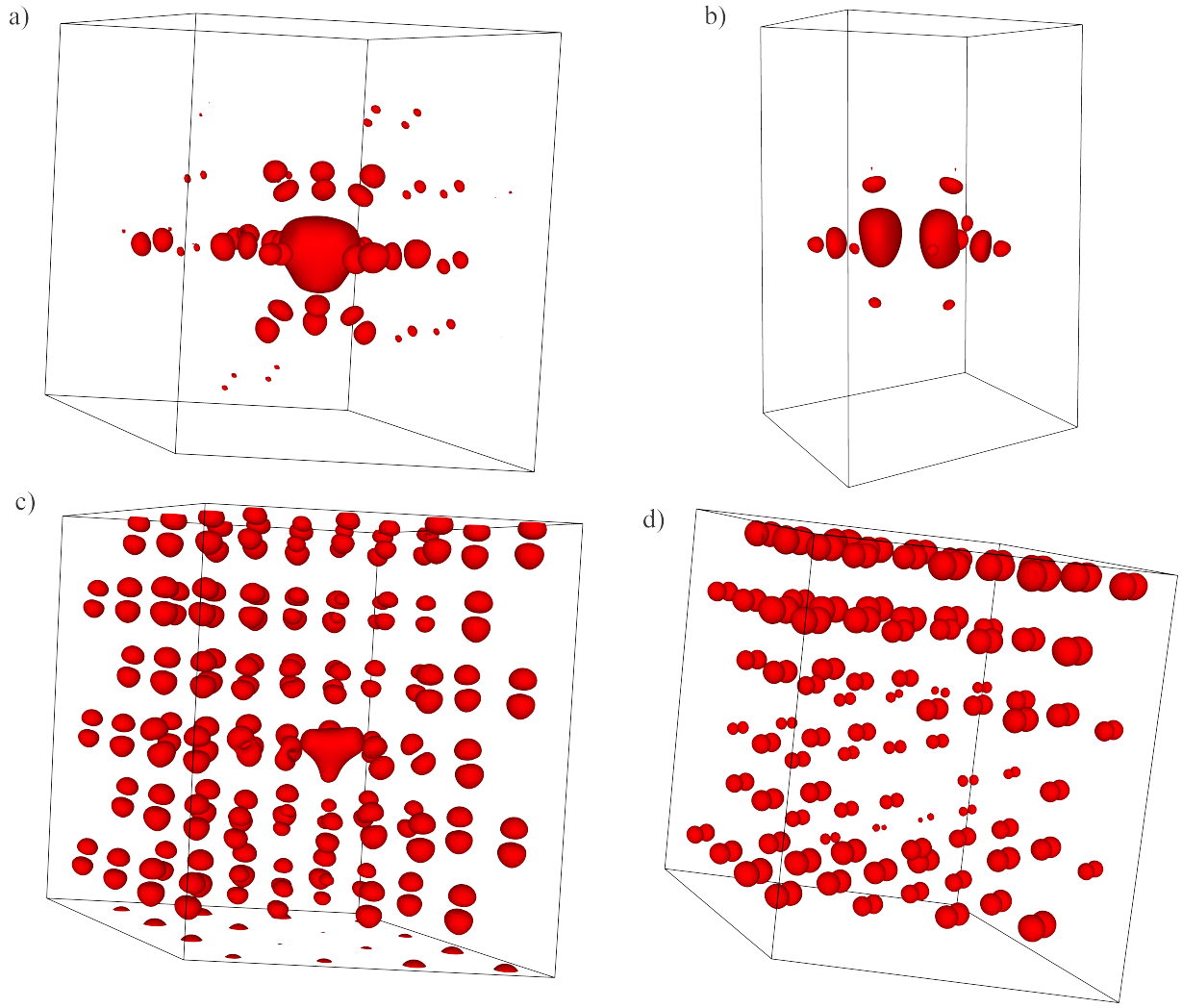

FIG. 2. Sample electronic charge density distributions predicted for bulk GaN with one V_N^{1+} defect. (a) s-like defect-centered; (b) p-like defect-centered; (c) bulk-defect hybrid; and (d) bulk-like orbitals. The k-point of all orbitals shown is (0.375, 0.625, 0.875) in crystal coordinates.

In order to create a systematic definition of the localized defect state, we developed Equation (1) to quantify the spatial extent of each orbital as the average distance of the electron density from the defect,

$$\langle \mathbf{r} \rangle = \frac{\int \|\mathbf{r} - \mathbf{r}_\mathbf{d}\| \rho(\mathbf{r}) dr^3}{\int \rho(\mathbf{r}) dr^3}. \qquad (1)$$

Here, $\mathbf{r}_d$ is the position of the vacancy, ρ is the charge density, and the integral is taken over the entire supercell volume. Using Equation (1), we classified, in an automated fashion, the spatial extent of the thousands of energy states that were calculated. To confirm this classification we also visually inspected the charge density for orbitals near the band gap (with orbitals plotted at an isosurface enclosing 50% of the total density).

The charge distribution of the defect state is slightly more delocalized with use of DFT-LDA for geometry optimization or electronic structure calculation. This observation along with the apparent over-binding present in the LDA-predicted lattice constants is consistent with the tendency of the LDA functional to delocalize the charge density and overbind atoms relative to hybrid functionals[90]. The calculated value for $\langle \mathbf{r} \rangle$ is on average 3.8-4.0 Å for the LDA-optimized geometry and 3.2-3.4 Å for the HSE30%-optimized geometry for the occupied s-type state, and 3.1-3.3 Å for both geometries for the lowest energy unoccupied p-type state (labeled p1), as presented in Table III. For comparison, the average $\langle \mathbf{r} \rangle$ for bulk-like states is approximately 7 Å, making it relatively straightforward to identify the defect orbitals from $\langle \mathbf{r} \rangle$. This analysis enables us to predict defect states that agreed with visual inspection every time.

TABLE III. Average value of the defect orbital spatial extent, $\langle \mathbf{r} \rangle$ computed from Eq. 1 for both the occupied s-like and the lowest energy unoccupied p-like defect state (p1). For each combination of geometry and DFT functional, the averages are based on approximately 64 orbitals.

Functional used for Geometry Optimization	Electronic Structure Method	Occupied s-type State $\langle \mathbf{r} \rangle$ [Å]	Unoccupied p-1 State $\langle \mathbf{r} \rangle$ [Å]
LDA	LDA	4.0	3.2
LDA	HSE06	3.4	3.1
HSE30%	LDA	3.8	3.3
HSE30%	HSE30%	3.2	3.3

B. Minimization of Defect-Defect Interactions

GaN has a relatively weak dielectric screening ($\epsilon_{r,\infty} = 4.9$; $\epsilon_{r,0} = 9.1$ as calculated by DFT-HSE30%) and therefore, the screening length in response to external electronic perturbations will be large. Hence, it is to be expected that the interaction of the defect with its periodic image will be significant, particularly for the case of the charged defect of the present study. To understand and minimize defect-defect interactions, we calculate the quasiparticle energy of the highest occupied and lowest unoccupied defect states for increasing supercell size using the GW method. We considered three n x n x m supercell sizes, with {(n,m) = (3,2); (4,3); (6;4)} as shown in Fig. 3(a). The smallest (greatest) distance between periodic images of the defect varies from 9.7 Å (10.6 Å) to 12.8 Å (15.6 Å) to 19.5 Å (21.1 Å) for (3,2), (4,3), and (6,4) respectively. Due to the computational cost associated with the largest supercell considered, these calculations are performed using a 1x1x1 Γ-centered k-point grid. As shown in Fig. 3(b), as the supercell size is increased from (3,2) to (6,4), the energy of the defect state converges to 0.1 eV for the one occupied and lowest unoccupied defect state and 0.2 eV for the higher-lying unoccupied defect states. Therefore, our final calculations use the 191-atom, 4 x 4 x 3 supercell.

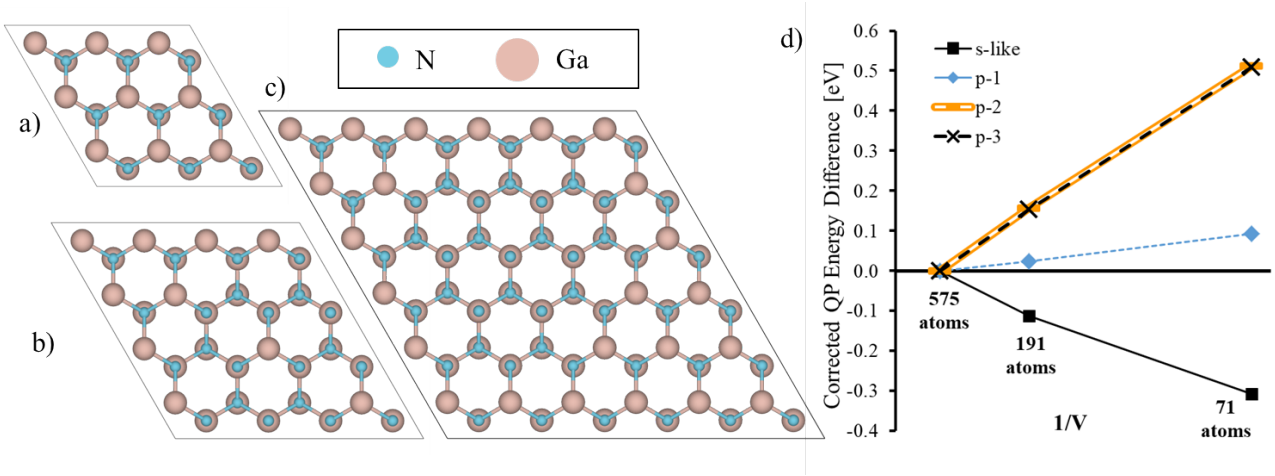

FIG. 3. (a)-(c) The GaN supercells containing one single charged N vacancy considered in this work. The number of replicated unit cells and associated number of atoms in parentheses are respectively (a) 3x3x2 (71 atoms), (b) 4x4x3 (191 atoms) and (c) 6x6x4 (575 atoms). The perspective is perpendicular to the crystallographic c axis. (d) The GW-calculated quasiparticle defect energies with respect to these supercell sizes, including charged supercell electrostatic correction of Eq. 2.

To further reduce the error of our calculations, we correct for the long-ranged charged defect-defect interactions, which has been noted in previous DFT-based studies[91]. We address these interactions by 1) a judicious choice of k-point mesh and 2) application of an electrostatic correction to defect-state eigenvalues.

The dependence of defect-defect interactions on the k-point mesh was first noted in the foundational work by Makov and Payne[92]. Using a tight binding argument, it was shown that interactions are largest at the Γ-point (k=**0**) and reduced for k-points away from Γ due to hybridization of the defect orbital. In this work, we utilize a 4x4x4 k-point grid shifted away from the Γ-point by (0.5 0.5 0.5). As explained in Section II, a 2x2x2 shifted grid is sufficient to converge the total energy to 1 meV/atom; however, we find that a denser k-point grid of 4x4x4 is necessary to describe the bulk-like states. Therefore, we utilize a 4x4x4 shifted grid for HSE calculations and interpolate the GW eigenvalues from a 2x2x2 to a 4x4x4 shifted grid using the Delaunay interpolation implemented in the BerkeleyGW package[93].

In addition, all defect state energies as defined by Fig. 2(a-b) were corrected for spurious electrostatic effects using Equation (2)[59,94] as implemented in the SXDEFECTALIGN software[95],

$$Ú_{d,corr} = -\frac{2}{q} E_{corr}, \qquad (2)$$

where E_{corr} is the total electrostatic energy correction proposed by Freysoldt, Neugebauer and Van de Walle[96,97] and q is the charge state of the defect. This procedure is necessary to correct for the errors in defect state energies due to the charged defect interacting with its periodic replicas, as well as the compensating background charge used in our DFT calculations[59,60,94].

Although the correction defined above greatly reduces the defect-defect interactions in the supercell, we find additional defect-defect interactions as evidenced by the k-point dispersion present in the defect state energy. It is expected that an isolated defect state will be dispersion-less (i.e., its energy will not vary with change in k-points). However, for the 4x4x3 supercell, we do find a dispersion of approximately 0.1 eV for the s-like defect state and 0.3 eV for the individual p-like states at both the DFT-HSE and GW level as shown in Table IV, suggesting defect-defect hybridization even with a shifted k-grid.

TABLE IV. The energy dispersion of the defect state for a 4x4x3 GaN supercell containing one V_N^{1+}. The occupied s-like defect state, minimum energy unoccupied and maximum energy unoccupied p-like defect states, referred to as p-1 and p-3 respectively, are shown for different geometries and levels of theory. The dispersion for a particular defect state is determined as the energy variation of that state over 64 k-points.

Functional used for Geometry Optimization	Electronic Structure Method	Defect State Dispersion [eV]		
		s-like	p-1	p-3
LDA	GW	0.08	0.37	0.29
LDA	DFT HSE06	0.13	0.26	0.23
HSE30%	GW	0.11	0.27	0.30
HSE30%	DFT HSE30%	0.16	0.27	0.26

In order to eliminate this error on the predicted defect state or trap energy, we define the energy as a weighted average over k-points using Equation (3)[94],

$$\overline{E_d^C} = \frac{\sum_N w_N E_d^C(N)}{\sum_N w_N}, \tag{3}$$

where N runs over all k-points, w_N is the associated k-point weight, and E_d^C is the energy of a particular defect state (e.g. occupied s-like). Equation (3) provides an accurate description of the defect state within DFT-LDA, for which we can check against the larger supercell size. The DFT-LDA dispersion is 0.1-0.3 eV for the 4x4x3 supercell, similar to GW and DFT-HSE, and is reduced to ~0.01 eV for the 6x6x4 supercell, indicating the presence of residual defect-defect interactions for the smaller supercell. However, averaging as with Equation (3) results in both occupied and unoccupied defect state energies that agree to 0.01 eV between 4x4x3 and 6x6x4 supercells, indicating that the average energy state is well-described by this procedure.

III.3. Role of the Underlying Geometry and Level of Theory on Predicted V_N^{1+} Trap State Energies

To better understand how quantitatively accurate defect state energies may be obtained, we investigate the role of underlying approximations on the predicted defect energy states. Fig. 4 shows the density of states (DOS) associated with the pristine and with-defect structure within the GW and DFT-HSE30% approximations, with geometry optimization via either DFT-LDA or DFT-HSE30%[87]. Here, we compare to the pristine bulk using the same k-point density and computational parameters as the with-defect studies.

All four calculations qualitatively agree in the general features of the defect structure: the introduction of the defect results in low-energy localized states; one occupied state contained within the valence band and a series of unoccupied states that constitute a peak in the DOS very near in energy to the bulk conduction band minimum. There is a k-point dispersion of ~0.1 eV for the occupied and 0.3-0.4 eV for the unoccupied defect states, which, as noted in Section III.2, is due to the defect-defect interactions of the periodic supercell. With three p-like states, this results in a spread of defect energies on the order 0.4-0.5 eV (prior to broadening) within the conduction band as shown in the insets of Fig. 4. Additionally, comparison of bulk and with-defect DOS suggests that our computational parameters are sufficient to describe bulk-like states accurately. For all four panels, the two DOS plots coincide closely at energies approximately 1 eV above the conduction band edge.

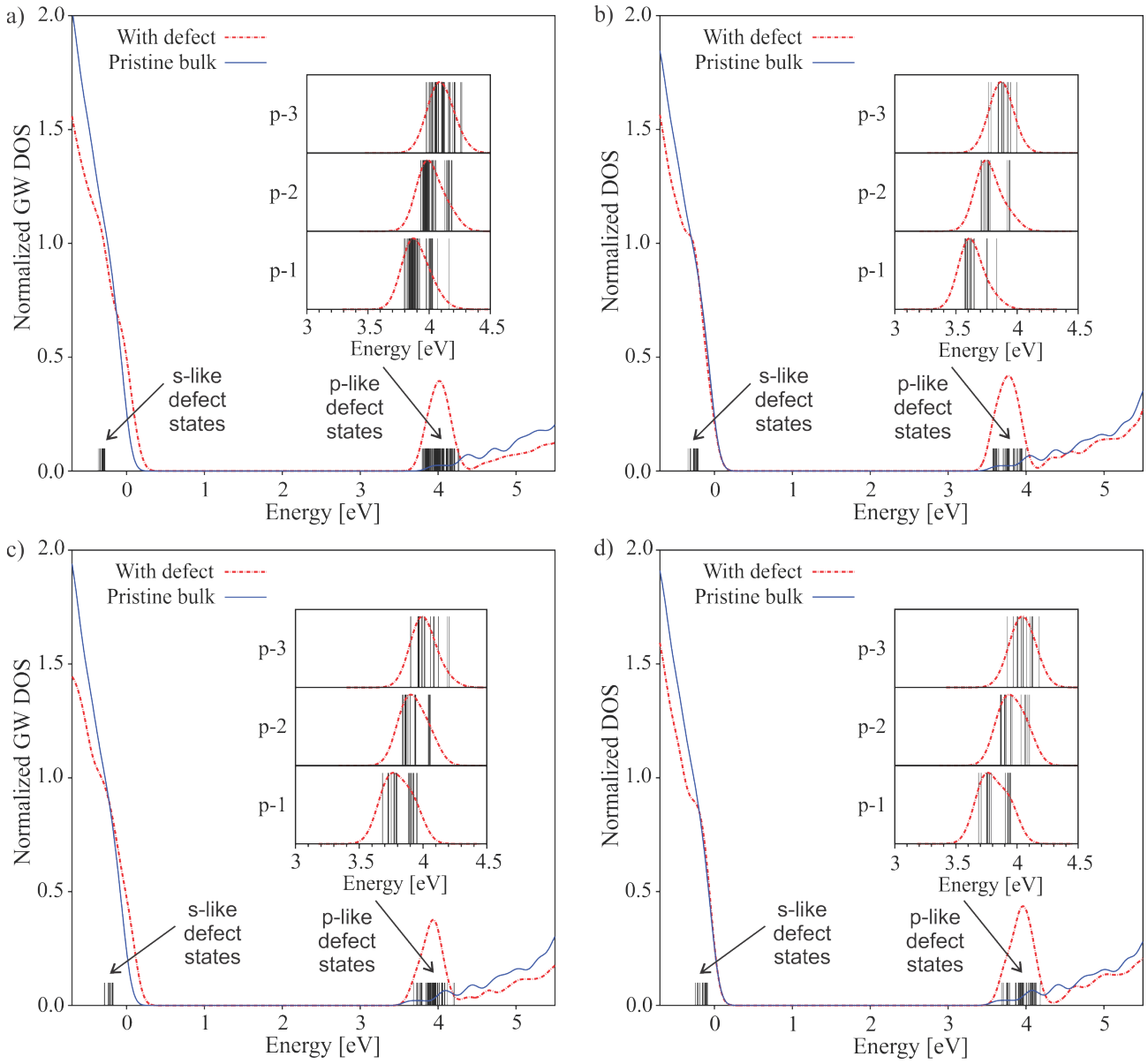

FIG. 4. The calculated density of states for pristine and with-V_N^{+1} bulk GaN for (a) GW, DFT-LDA geometry (b) DFT-HSE06, DFT-LDA geometry, (c) GW, DFT-HSE30% geometry and (d) DFT-HSE30%, DFT-HSE30% geometry. For b), DFT-HSE06 predicts the experimental band gap and was therefore used. The VBM of all bulk DOS datasets are shifted to zero and the quasiparticle and KS-DFT eigenvalues are broadened by a Gaussian function of width 0.2 eV. Black vertical lines show the energies of defect states.

Importantly, as was found for the pristine bulk, the predicted defect state energies agree well for DFT-HSE and GW, as long as the geometry is kept constant (comparison of Figs. 4(a) and 4(b) or Figs. 4(c) and 4(d). The density of valence states agree very well between the two structures and the density of conduction states agree in shape and peak positions to ~0.1 eV beyond the first defect-centered peak. With change in geometry however, the bulk band gap is modified and defect energies are shifted with respect to band edges (comparison of Figs. 4a and 4c or Figs. 4b and 4d). In particular, with a DFT-LDA-optimized geometry, the unoccupied defect states are at or below the bulk conduction band minimum (Figs. 4a and 4b), while the HSE30%-optimized geometry results in unoccupied defect states that are well within the conduction band by a few 0.1 eV.

III.4. Quantitatively Accurate Defect State Energies: Summary of Results

A. The trap state energy

We summarize the results of our calculations in Fig. 5 with schematic band-diagrams that illustrate the predicted trap state energy associated with each defect, computed via Eq. (3), and its position with respect to the band-edges. All levels of theory predict that the states associated with the defects are low-lying (close to the band edges). However, the exact position with respect to band edges can vary by as much as 0.2 eV with different approximations, with most of the discrepancy due to different geometries. With DFT-LDA-optimized geometry, GW predicts that the s-like occupied state is 0.3 eV below the VBM and the lowest energy p-like unoccupied state is at 0.02 eV below the CBM. With the DFT-HSE30%-optimized geometry, this position changes to 0.2 eV below the VBM for the occupied state and 0.2 eV above the CBM for the lowest energy unoccupied state. As was found for the bulk, when the geometry is fixed, GW and DFT-HSE30% agree on average to within 0.05 eV or better in predicted energetics. We note here that our predictions regarding trap state energies do not include the effects of geometry relaxation.

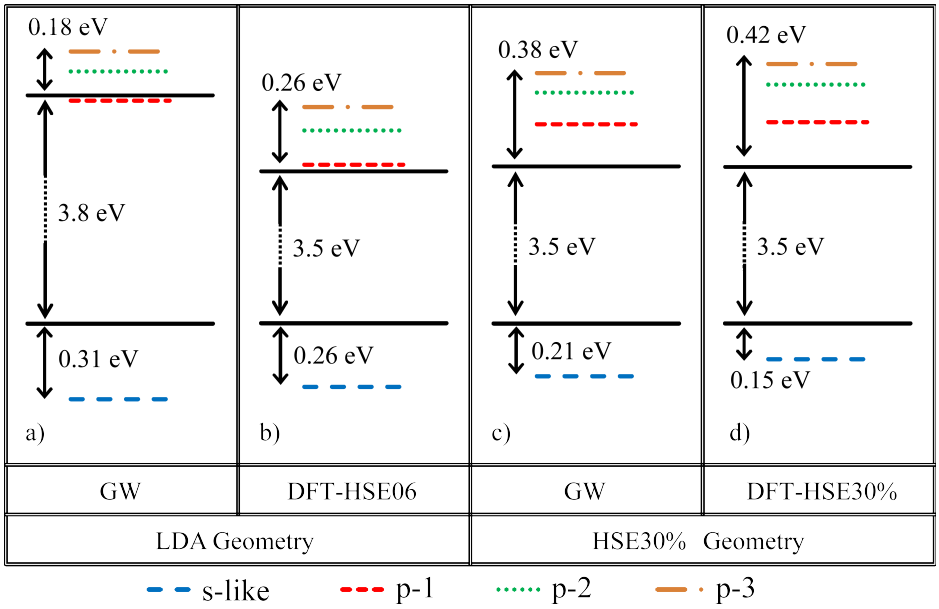

FIG. 5. The calculated defect state energy for both the occupied s-like unoccupied p-like defect state relative to the VBM and CBM, respectively determined using (a) GW with DFT-LDA geometry, (b) DFT-HSE06 with DFT-LDA geometry, (c) GW with DFT-HSE30% geometry and (d) DFT-HSE30% with DFT- HSE30% geometry.

The change in the predicted trap state energy with geometry can result in very different conclusions about electron transport within this structure. With use of the DFT-LDA geometry, the prediction of trap-state energies at the bottom of the conduction band, the defect would play a more destructive role, as a carrier trapping and scattering center, whereas a state 0.2 eV above the conduction band predicted when utilizing the DFT-HSE geometry is sufficiently high in energy (>> k_BT) such that it would be benign towards carriers. Since HSE30% results in the best agreement of geometry with experiment for pristine bulk, we expect that this geometry will provide the best description of the defect state and that the V_N^{1+} defect will not act as a trap to carriers in GaN. We note that the defect state energies predicted via the analysis of quasiparticle energies agree qualitatively with thermodynamic transition energy levels predicted by previous studies[12,39,65,98–100]. Specifically, the thermodynamic transition level $\varepsilon(+1/0)$, which corresponds to our calculated lowest energy p-type state, is predicted to be slightly below (~0.5 eV) to slightly above (~0.2 eV) the conduction-band minimum[65,100]. Exact agreement is not to be expected since we calculate the energies associated with addition and removal

of electrons from the defect, and the thermodynamic transition levels describe the phase transition energies between different charged states. However, since both analyses do describe energetics associated with charging a defect, we expect and find qualitative agreement.

B. Error Bars Associated with GW Calculation

Our study has shown that analysis of the quasiparticle spectrum associated with a defective crystal provides a rich set of information such as the energy states associated with multiple defect states, their position with respect to band edges, and defect-defect interactions for closely spaced defects. However, these properties, particularly the energy states, are difficult to converge. Our thorough analysis of computational methods and approximations provides an estimate of the error bars associated with these defect-focused calculations.

Assuming a low defect density in the bulk, the largest source of error in our calculations is introduced by the use of a periodically repeating supercell, which results in defect-defect interactions, as evidenced by the large defect energy state dispersion. In this work, with a 191-atom, 4x4x3 supercell, the error ranges from 0.1 eV for the occupied to 0.3 eV for the unoccupied defect states. However, as noted in Section III.1.B, the error associated with the average value of the calculated defect state is one order of magnitude smaller. The calculated dispersion suggests that there is hybridization of the defect states with their periodic images, particularly the p-type unoccupied orbitals. Thus, at an average separation between defect and its periodic image along all directions of 13.7 Å in our system, we anticipate significant delocalization of the defect states such that there is density overlap between neighboring states and hybridization. This suggests that there may be additionally errors associated with the point-charge-like electrostatic correction for defect interactions that we utilize in Equation (2).

Additional sources of error include the GW convergence error which is estimated to be negligible here at ~0.01 eV, due to the convergence of our parameters, and the error introduced by the limited supercell size (excluding dispersion) which we calculate to be ~ 0.1- 0.2 eV depending on the defect state. Lastly, the underlying geometry can introduce errors of tenths of eVs, as is the case for the bulk band gap.

Importantly, our calculations also indicate that tuned DFT-HSE agrees to better than 0.1 eV with the GW approximation, suggesting that tuning the fraction of Hartree-Fock exchange for the bulk provides a balance of exchange and correlation that is accurate when comparing to accurate electron-electron interactions determined via many-body perturbation theory.

IV. Conclusions

In conclusion, we have applied first-principles theory to quantitatively describe the energy states associated with the +1 charged nitrogen vacancy within bulk GaN as a prototypical defective material. We developed a rigorous approach for describing and classifying the defect state and by analysis of the accuracy of our calculations, estimated an error of a few tenths of eV in predicting energy states with respect to band edges. We predict that both Kohn-Sham eigenvalues obtained from tuned DFT-HSE and quasiparticle energies obtained from the GW approximation agree well in the predicted value of occupied and unoccupied defect state energies, with both indicating that the +1 charged N-vacancy will not act as a trap state for carriers. Additionally, we predict that the level of theory with which the atomic structure is optimized strongly impacts the predicted eigenvalues, due to the ionic nature of the Ga-N bond. For the pristine bulk, tuned DFT-HSE results in the best agreement of geometry with experiment; therefore, we consider the best estimate for the defect energy states are those from the DFT-HSE geometry placing the occupied defect state at 0.2 eV below the VBM and the lowest energy unoccupied defect state at 0.2 eV above the CBM for this particular vacancy. We propose that a quasiparticle analysis of defect energy states will provide new understanding of the energetics associated with defects and complement existing approaches to calculate thermodynamic transition levels.

ACKNOWLEDGMENTS

D.K.L and S.S. thank Jan Andzelm at the U.S. Army Research Laboratory for helpful discussions. The authors gratefully acknowledge the financial support from the U.S. Army Research Laboratory through the Collaborative Research Alliance (CRA) under Grant No. W911NF-12–2-0023 for MultiScale Multidisciplinary Modeling of Electronic Materials (MSME). D.K.L and S.S. gratefully acknowledge funding from Boston University. Additionally, we acknowledge grants of computer time from the U.S. Army Research Laboratory, the National Energy Research Scientific Computing Center, a DOE Office of Science User Facility supported by the Office of Science of the U.S. Department of Energy under Contract No. DE-AC02-05CH11231, and the Extreme Science and Engineering Discovery Environment (XSEDE)[101] which is supported by National Science Foundation grant number ACI-1548562. In addition this research used resources of the Boston University Scientific Computing Center at the Massachusetts Green High-Performance Computing Center (MGHPCC).

---

[1] A.H. Wilson, Proc. R. Soc. London A Math. Phys. Eng. Sci. **134**, 277 (1931).

[2] S.T. Pantelides, Rev. Mod. Phys. **50**, 797 (1978).

[3] G.A. Baraff, Philos. Trans. R. Soc. London A Math. Phys. Eng. Sci. **341**, 195 (1992).

[4] E.R. Weber, Phys. B Condens. Matter **340**, 1 (2003).

[5] M.G. Ganchenkova and R.M. Nieminen, Phys. Rev. Lett. **96**, 196402 (2006).

[6] E.G. Seebauer and M.C. Kratzer, *Charged Semiconductor Defects: Structure, Thermodynamics and Diffusion* (Springer-Verlag, London, 2009).

[7] E.G. Seebauer and M.C. Kratzer, Mater. Sci. Eng. R Reports **55**, 57 (2006).

[8] S. Sasaki, K. Kawahara, G. Feng, G. Alfieri, and T. Kimoto, J. Appl. Phys. **109**, 13705 (2011).

[9] N. Iwamoto and B.G. Svensson, in *Defects Semicond.*, 1st ed. (Academic Press, 2015), pp. 369–407.

[10] D.C. Look, Phys. Status Solidi B Basic Res. **228**, 293 (2001).

[11] P.A. Schultz and A.H. Edwards, Nucl. Instruments Methods Phys. Res. B **327**, 2 (2014).

[12] C.G. Van de Walle and J. Neugebauer, J. Appl. Phys. **95**, 3851 (2004).

[13] S. Wei, S.B. Zhang, and A. Zunger, **87**, 1304 (2000).

[14] J. Coutinho, R. Jones, P.R. Briddon, and S. Oberg, Phys. Rev. B **62**, 10824 (2000).

[15] S. Goedecker, T. Deutsch, and L. Billard, Phys. Rev. Lett. **88**, 235501 (2002).

[16] R.J. Needs, J. Phys. Condens. Matter **11**, 10437 (1999).

[17] C.G. Van De Walle, P.J.H. Denteneer, Y. Bar-Yam, and S.T. Pantelides, Phys. Rev. B **39**, 10791 (1989).

[18] D.J. Chadi and K.J. Chang, Phys. Rev. Lett. **61**, 873 (1988).

[19] J. Dabrowski and M. Scheffler, Phys. Rev. Lett. **60**, 2183 (1988).

[20] T. Mattila and R.M. Nieminen, Phys. Rev. B **54**, 16676 (1996).

[21] J. Dabrowski and M. Scheffler, Phys. Rev. B **40**, 10391 (1989).

[22] S.B. Zhang and J.E. Northrup, Phys. Rev. Lett. **67**, 2339 (1991).

[23] J.E. Northrup and S.B. Zhang, Phys. Rev. B **47**, 6791 (1993).

[24] J.E. Northrup and S.B. Zhang, Phys. Rev. B **50**, 4962 (1994).

[25] K. Laasonen, R.M. Nieminen, and M.J. Puska, Phys. Rev. B **45**, 4122 (1992).

[26] J. Neugebauer and C.G. Van De Walle, Phys. Rev. B **50**, 8067 (1994).

[27] A. Stroppa and G. Kresse, Phys. Rev. B **79**, 201201 (2009).

[28] J.L. Lyons, A. Janotti, and C.G. Van de Walle, Appl. Phys. Lett. **97**, 152108 (2010).

[29] J.L. Lyons, A. Janotti, and C.G. Van De Walle, Phys. Rev. Lett. **108**, 156403 (2012).

[30] C.G. Van de Walle, Phys. Rev. B **56**, R10020 (1997).

[31] M. Matsubara and E. Bellotti, J. Appl. Phys. **121**, 195701 (2017).

[32] A. Kyrtsos, M. Matsubara, and E. Bellotti, Phys. Rev. B **93**, 245201 (2016).

[33] M. Matsubara and E. Bellotti, J. Appl. Phys. **121**, 195702 (2017).

[34] E. Bellotti, F. Bertazzi, S. Shishehchi, M. Matsubara, and M. Goano, IEEE Trans. Electron Devices **60**, 3204 (2013).

[35] J.P. Perdew, Int. J. Quantum Chem. **28**, 497 (1985).

[36] J. Kohanoff, *Electronic Structure Calculations for Solids and Molecules* (Cambridge University Press, Cambridge, 2006).

[37] J. Heyd, G.E. Scuseria, and M. Ernzerhof, J. Chem. Phys. **118**, 8207 (2003).

[38] J. Heyd, J.E. Peralta, G.E. Scuseria, and R.L. Martin, J. Chem. Phys. **123**, 174101 (2005).

[39] M.A. Reshchikov, D.O. Demchenko, J.D. McNamara, S. Fernández-Garrido, and R. Calarco, Phys. Rev. B **90**, 35207 (2014).

[40] G. Mattioli, P. Alippi, F. Filippone, R. Caminiti, and A. Amore Bonapasta, J. Phys. Chem. C **114**, 21694 (2010).

[41] S.J. Clark, J. Robertson, S. Lany, and A. Zunger, Phys. Rev. B **81**, 115311 (2010).

[42] A. Janotti, J.B. Varley, P. Rinke, N. Umezawa, G. Kresse, and C.G. Van de Walle, Phys. Rev. B **81**, 85212 (2010).

[43] D.M. Hofmann, D. Kovalev, G. Steude, B.K. G Meyer, A. Hoffmann, L. Eckey, R. Heitz, T. Detchprom, H. Amano, and I. Akasaki, Phys. Rev. B **52**, 16702 (1995).

[44] D.O. Demchenko, I.C. Diallo, and M.A. Reshchikov, Phys. Rev. Lett. **110**, 87404 (2013).

[45] A. Alkauskas and A. Pasquarello, Phys. Rev. B - Condens. Matter Mater. Phys. **84**, 125206 (2011).

[46] A. Alkauskas, P. Broqvist, and A. Pasquarello, Phys. Status Solidi B **248**, 775 (2011).

[47] J.R. Weber, A. Janotti, and C.G. Van De Walle, J. Appl. Phys. **109**, 33715 (2011).

[48] R. Ramprasad, H. Zhu, P. Rinke, and M. Scheffler, Phys. Rev. Lett. **108**, 66404 (2012).

[49] S. Lany and A. Zunger, Model. Simul. Mater. Sci. Eng. **17**, 84002 (2009).

[50] L. Hedin, Phys. Rev. **139**, A796 (1965).

[51] L. Hedin and S. Lundqvist, Solid State Phys. **23**, 1 (1970).

[52] M.S. Hybertsen and S.G. Louie, Phys. Rev. B **34**, 5390 (1986).

[53] P. Rinke, A. Janotti, M. Scheffler, and C.G. Van de Walle, Phys. Rev. Lett. **102**, 26402 (2009).

[54] F. Bruneval and G. Roma, Phys. Rev. B **83**, 144116 (2011).

[55] M. Hedstrom, A. Schindlmayr, G. Schwarz, and M. Scheffler, Phys. Rev. Lett. **97**, 226401 (2006).

[56] L. Martin-Samos, G. Roma, P. Rinke, and Y. Limoge, Phys. Rev. Lett. **104**, 75502 (2010).

[57] W. Chen and A. Pasquarello, **96**, 20101 (2017).

[58] S. Lany and A. Zunger, Phys. Rev. B **81**, 113201 (2010).

[59] M. Jain, J.R. Chelikowsky, and S.G. Louie, Phys. Rev. Lett. **107**, 216803 (2011).

[60] A. Malashevich, M. Jain, and S.G. Louie, Phys. Rev. B **89**, 75205 (2014).

[61] F. Bruneval, Nucl. Instruments Methods Phys. Res. Sect. B **277**, 77 (2012).

[62] W. Chen and A. Pasquarello, J. Phys. Condens. Matter **27**, 133202 (2015).

[63] M.L. Tiago and J.R. Chelikowsky, Phys. Rev. B - Condens. Matter Mater. Phys. **73**, 205334 (2006).

[64] G.D. Chen, M. Smith, J.Y. Lin, H.X. Jiang, M.A. Khan, and C.J. Sun, Appl. Phys. Lett. **67**, 1653 (1995).

[65] C. Lyons, John L Van de Walle, NPJ Comput. Mater. **3**, 1 (2017).

[66] S. Tomiya, in *Mater. Reliab. Handb. Semicond. Opt. Electron Devices* (Springer, New York, 2013), pp. 207–245.

[67] M.A. Reshchikov and H. Morkoc, J. Appl. Phys. **97**, 61301 (2005).

[68] D.M. Ceperley and B.J. Alder, Phys. Rev. Lett. **45**, 566 (1980).

[69] J. Paier, M. Marsman, K. Hummer, G. Kresse, I.C. Gerber, and J.G. Angyán, J. Chem. Phys. **124**, 154709 (2006).

[70] M. Leslie and N.J. Gillan, J. Phys. C Solid State Phys. **18**, 973 (1985).

[71] G. Kresse, Phys. Rev. B **54**, 11169 (1996).

[72] G. Kresse, Phys. Rev. B **59**, 1758 (1999).

[73] P. Giannozzi, S. Baroni, N. Bonini, M. Calandra, R. Car, C. Cavazzoni, D. Ceresoli, G.L. Chiarotti, M. Cococcioni, I. Dabo, A. Dal Corso, S. de Gironcoli, S. Fabris, G. Fratesi, R. Gebauer, U. Gerstmann, C. Gougoussis, A. Kokalj, M. Lazzeri, L. Martin-Samos, N. Marzari, F. Mauri, R. Mazzarello, S. Paolini, A. Pasquarello, L. Paulatto, C. Sbraccia, S. Scandolo, G. Sclauzero, A.P. Seitsonen, A. Smogunov, P. Umari, and R.M. Wentzcovitch, J. Physics. Condens. Matter **21**, 395502 (2009).

[74] P.E. Blöchl, Phys. Rev. B **50**, 17953 (1994).

[75] N. Troullier and J.L. Martins, Phys. Rev. B **43**, 1993 (1991).

[76] S.G. Louie, S. Froyen, and M.L. Cohen, Phys. Rev. B **26**, 1738 (1982).

[77] J. Deslippe, G. Samsonidze, M. Jain, M.L. Cohen, and S.G. Louie, Phys. Rev. B **87**, 165124 (2013).

[78] J.E. Moussa, P.A. Schultz, and J.R. Chelikowsky, J. Chem. Phys. **136**, 204117 (2012).

[79] B. Monemar, Phys. Rev. B **10**, 676 (1974).

[80] A. Polian, M. Grimsditch, and I. Grzegory, J. Appl. Phys. **79**, 3343 (1996).

[81] S. Limpijumnong and C. Van de Walle, Phys. Rev. B **69**, 35207 (2004).

[82] M.S. Hybertsen and S.G. Louie, Phys. Rev. Lett. **55**, 1418 (1985).

[83] J. Deslippe, G. Samsonidze, D.A. Strubbe, M. Jain, M.L. Cohen, and S.G. Louie, Comput. Phys. Commun. **183**, 1269 (2012).

[84] G. Samsonidze, C.-H. Park, and B. Kozinsky, J. Phys. Condens. Matter **26**, 475501 (2014).

[85] J. Lischner, S. Sharifzadeh, J. Deslippe, J.B. Neaton, and S.G. Louie, Phys. Rev. B **90**, 115130 (2014).

[86] G. Samsonidze, M. Jain, J. Deslippe, M.L. Cohen, and S.G. Louie, Phys. Rev. Lett. **107**, 186404 (2011).

[87] See Supplemental Material at [] for further details of GW calculations and a with-defect band structure.

[88] J.P. Perdew, K. Burke, and M. Ernzerhof, Phys. Rev. Lett. **77**, 3865 (1996).

[89] G.L. Pikus and G.E. Bir, *Symmetry and Strain-Induced Effects in Semiconductors* (Wiley, New York, 1974).

[90] A. Carvalho, A. Alkauskas, A. Pasquarello, A.K. Tagantsev, and N. Setter, Phys. Rev. B **80**, 195205 (2009).

[91] S. Lany and A. Zunger, Phys. Rev. B **78**, 235104 (2008).

[92] G. Makov, R. Shah, and M. Payne, Phys. Rev. B **53**, 15513 (1996).

[93] Computer code BerkeleyGW available at www. berkeleygw.org (2017).

[94] W. Chen and A. Pasquarello, Phys. Rev. B **88**, 115104 (2013).

[95] C. Freysoldt, Computer code SXDEFECTALIGN available at https://sxrepo.mpie.de/projects/sphinx-add-ons/files (2017).

[96] C. Freysoldt, J. Neugebauer, and C.G. Van de Walle, Phys. Status Solidi B **248**, 1067 (2011).

[97] C. Freysoldt, J. Neugebauer, and C.G. Van de Walle, Phys. Rev. Lett. **102**, 16402 (2009).

[98] Q. Yan, A. Janotti, M. Scheffler, and C.G. Van De Walle, Appl. Phys. Lett. **100**, 142110 (2012).

[99] I.C. Diallo and D.O. Demchenko, Phys. Rev. Appl. **6**, 64002 (2016).

[100] G. Miceli and A. Pasquarello, Phys. Rev. B **93**, 165207 (2016).

[101] J. Towns, T. Cockerill, M. Dahan, I. Foster, K. Gaither, A. Grimshaw, V. Hazlewood, S. Lathrop, D. Lifka, G. Peterson, R. Roskies, J.R. Scott, and N. Wilkins-Diehr, Comput. Sci. Eng. **16**, 62 (2014).

[102] J.P. Perdew and R. Norman, Phys. Rev. B **26**, 5455 (1982).